Pergamon

PII: S0306-4522(98)00315-7

Neuroscience Vol. 89, No. 2, pp. 347–362, 1999

0306–4522/99 $19.00+0.00

FAST BURST FIRING AND SHORT-TERM SYNAPTIC PLASTICITY: A MODEL OF NEOCORTICAL CHATTERING NEURONS

X.-J. WANG

Center for Complex Systems and Department of Physics, Brandeis University, Waltham, MA 02254, U.S.A.

Abstract—We present an ionic conductance model of chattering neurons in the neocortex, which fire fast rhythmic bursts in the gamma frequency range (~40 Hz) in response to stimulation [Gray C. M. and McCormick D. A. (1996) *Science* **274,** 109–113]. The bursting mechanism involves a "ping-pong" interplay between soma-to-dendrite back propagation of action potentials and an afterdepolarization generated by a persistent dendritic Na^+ current and a somatic Na^+ window current. The oscillation period is primarily determined by a slowly inactivating K^+ channel and passive membrane properties. The model behavior is compared quantitatively with the experimental data. It is shown that the cholinergic muscarinic receptor activation can transform the model cell's firing pattern from tonic spiking to rapid bursting, as a possible pathway for acetylcholine to promote 40-Hz oscillations in the visual cortex. To explore possible functions of fast burst firing in the neocortex, a hypothetical neural pair is simulated, where a chattering cell is presynaptic to an inhibitory interneuron via stochastic synapses. For this purpose, we use a synapse model endowed with a low release probability, short-term facilitation and vesicle depletion. This synapse model reproduces the behavior of certain neocortical pyramid-to-interneuron synapses [Thomson A. M. *et al.* (1993) *Neuroscience* **54,** 347–360]. We showed that the burstiness of cell firing is required for the rhythmicity to be reliably transmitted to the postsynaptic cell via unreliable synapses, and that fast burst firing of chattering neurons can provide an exceptionally powerful drive for recruiting feedback inhibition in cortical circuits.

From these results, we propose that the fast rhythmic burst firing of neocortical chattering neurons is generated by a calcium-independent ionic mechanism. Our simulation results on the neural pair highlight the importance of characterizing the short-term plasticity of the synaptic connections made by chattering cells, in order to understand their putative pacemaker role in synchronized gamma oscillations of the visual cortex. © 1998 IBRO. Published by Elsevier Science Ltd.

Key words: cortical gamma rhythm, chattering cells, short-term synaptic plasticity, acetylcholine modulation, biophysical model.

Synchronization of neuronal assemblies represents an attractive candidate *modus operandi* for cortical networks to integrate stimulus features into a sensory percept.[24,29,44] Synchronous firing of cortical neurons has been commonly observed in association with fast oscillatory discharges in the gamma (20–70 Hz) frequency range.[7,14,15,27,38,42] However, our search for computational implications of this phenomenon has been hindered by our lack of understanding of its underlying cellular and circuit mechanisms. For instance, although gamma ("40 Hz") oscillations have been widely reported in single-unit recordings or local field potentials from various cortical areas of both anesthetized and alert cats, monkeys and other animal species, we still do not know the precise state-dependent or perception-related conditions under which this rhythmicity is expected to occur, and how it may be controlled by modulatory signals from the brainstem reticular system.[37,47]

Abbreviations: ADP, afterdepolarization; $[Ca^{2+}]_i$, intracellular calcium concentration; EPSP, excitatory postsynaptic potential; IRIH, inter-release interval histogram; ISIH, inter-spike interval histogram.

In an *in vitro* slice preparation of the rat frontal cortex, Llinás *et al.*[28] described a subset of layer IV interneurons which, under current injection, displayed subthreshold oscillations in the gamma frequency range. Because the oscillatory membrane potentials were sensitive to tetrodotoxin, the authors concluded that the rhythmicity intrinsic to single neurons was produced by an interplay between a persistent Na^+ channel and an unspecified delayed rectifier K^+ channel. Such a mechanism has been demonstrated in a computer-simulated biophysical model, which suggests that the kinetic properties required for the 40-Hz rhythmogenesis may be fulfilled by a low-threshold, slowly-inactivating K^+ current.[62] More recently, Gray and McCormick[13] performed *in vivo* intracellular recordings from the cat visual cortex and found a subclass of pyramidal ("chattering") neurons in superficial layers II and III, which display prominent rhythmic bursting at 20–70 Hz in response to either visual stimulation or applied current pulses (see also Ref. 19). Each burst typically consists of two to four action potentials, and the intraburst firing rate is 300–500 Hz or

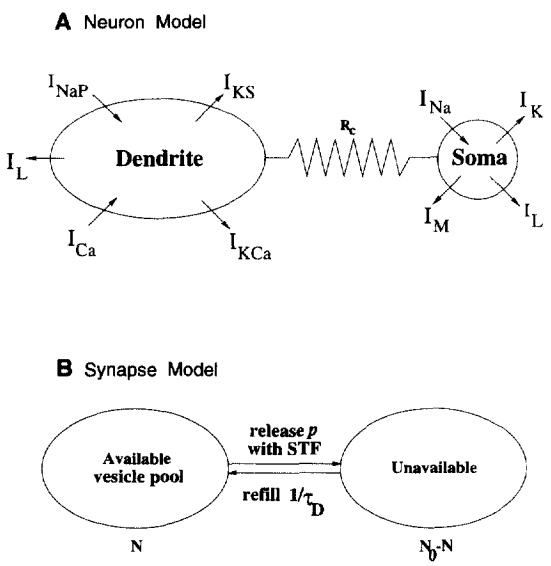

Fig. 1. Schematic two-compartment chattering neuron model (A) and stochastic synapse model with short-term facilitation and vesicle depletion (B). See Computational Procedures for detailed description.

higher.[13] Similar chattering behavior has been reported in certain pyramidal cells that project to outside of the neocortex.[4,46,48] Preliminary results from *in vitro* slice experiments indicate that the chattering behavior may depend on activation of muscarinic cholinergic receptors.[33]

In this paper, we report a computational work that addresses three questions raised by the findings of Gray and McCormick. (1) What are the ionic mechanisms for the fast rhythmic bursting behavior of the chattering neurons? (2) What is the cellular basis of cholinergic modulation of chattering firing patterns? (3) What may be the implications of such fast burst firing in the gamma rhythmogenesis of the visual cortex? We investigate these issues by proposing a biophysical model of chattering cells, and by simulating a hypothetical neural pair where a chattering cell drives an inhibitory interneuron via stochastic synapses endowed with short-term synaptic facilitation and vesicle depletion. A pacemaker neuron must be able to reliably transmit the rhythmicity to its postsynaptic targets. This is problematic in cortical networks, where synapses can be very unreliable, with low release probability p,[49,56] and there are only a few (often one) synaptic contacts between a cell pair.[21] Unreliable transmission can be made reliable by convergent inputs from several presynaptic cells. However, for a postsynaptic cell to receive a rhythmic drive through this mechanism, the oscillations in the presynaptic pacemaker neurons must be synchronized in time, an assumption which should not be taken for granted. It has been proposed that bursts may be advantageous for neural communication, by providing a reliable signal across low-p synapses[26] or by enhancing synaptic transmission through short-term facilitation.[22] Consistent with this view, our simulation results show that chattering cells are capable of acting as robust pacemaker for the 40-Hz oscillations in cortical networks, because their burst firing provides a reliable signal across low-p and facilitating synapses.

COMPUTATIONAL PROCEDURES

Chattering neuron model

Our minimal model includes only ion channels that are considered essential to the chattering behavior. As illustrated in Fig. 1A, the neuron model has two compartments, representing the dendrite and the soma (plus axonal initial segment), respectively.[31,39] The dendritic compartment has a persistent sodium current I_{NaP}, a slowly-inactivating potassium current I_{KS}, a high-threshold calcium current I_{Ca}, a slow calcium-dependent potassium current I_{KCa} and a leak current I_L. The somatic compartment contains spike-generating currents I_{Na} and I_K, an M-type potassium current I_M, and a leak current I_L.

The somatic and dendritic membrane potentials V_s and V_d obey the following current-balance equations:

$$C_m A_s dV_s/dt = -A_s(I_L+I_{Na}+I_K+I_M+I_{input})+I_{app}-(V_s-V_d)/R_c$$

$$C_m A_d dV_d/dt = -A_d(I_L+I_{NaP}+I_{KS}+I_{Ca}+I_{KCa}+I_{input})-(V_d-V_s)/R_c$$

where $C_m=1\ \mu F/cm^2$. The membrane surface areas are assumed to be $A_{tot}=A_s+A_d=33{,}000\ \mu m^2$ and $A_s/A_{tot}=0.15$. The axial resistance (coupling) $R_c=15\ M\Omega$. The cell is either excited by an injected current I_{app} (in nA) or a synaptic current I_{input} of the α-amino-3-hydroxy-5-methyl-4-isoxazolepropionate type: $I_{input}=g_{input}s(V-E_{input})$. The gating variable s obeys the equation $ds/dt=\eta(t)-s/\tau_s$, where $\eta(t)$ is a Poisson process with rate λ and the decay time $\tau_s=2$ ms.

Ion channel kinetics. The voltage-dependent currents are described by the Hodgkin–Huxley formalism. Thus, a gating variable x satisfies first-order kinetics, $dx/dt=\phi_x[\alpha_x(V)(1-x)-\beta_x(V)x]=\phi_x[x_\infty(V)-x]/\tau_x(V)$, where ϕ_x is the temperature factor. I_{NaP} and I_{KS} were taken from a previous model,[62] with slight change of parameter values. $I_{NaP}=g_{NaP}m_\infty(V-E_{Na})$, where its rapid activation was substituted by its steady-state $m_\infty(V)=1/[1+\exp[-(V+45)/5]]$.[11] The I_{KS} has a low activation voltage threshold and inactivates slowly:[45] $I_{KS}=g_{KS}mh(V-E_K)$, $m_\infty=1/[1+\exp[-(V+34)/6.5]]$, $\tau_m=\tau_0/[\exp[-(V+55)/30]+\exp[(V+55)/30]]$, $\tau_0=8$ ms; $h_\infty=1/[1+\exp[(V+65)/6.6]]$, $\tau_h=100/[1+\exp[-(V+65)/6.8]]+100$.

The high-threshold calcium current $I_{Ca}=g_{Ca}m^2{}_\infty(V-E_{Ca})$, where $m_\infty(V)=1/[1+\exp[-(V+20)/10]]$. The voltage-independent, calcium-activated potassium current $I_{KCa}=g_{KCa}m_{KCa}(V-E_K)$, with $m_{KCa}=[Ca^{2+}]_i/([Ca^{2+}]_i+D_K)$, $D_K=30\ \mu M$. The intracellular calcium concentration $[Ca^{2+}]_i$ is assumed to be governed by first-order kinetics: $d[Ca^{2+}]_i/dt=-\alpha I_{Ca}-[Ca^{2+}]_i/\tau_{Ca}$, where $\alpha=0.002$ and $\tau_{Ca}=200$ ms.

The spike-generating currents are adopted from Hodgkin and Huxley,[16] with faster kinetics so that the spikes are brief (duration of 0.3 ms at half-amplitude). The sodium current $I_{Na}=g_{Na}m^3h(V-V_{Na})$, where $\alpha_m=-0.1(V+32)/[\exp[-0.1(V+32)]-1]$, $\beta_m=4\exp[-(V+57)/18]$, $\alpha_h=0.07\exp[-(V+44)/20]$, $\beta_h=1/[\exp[-0.1(V+14)]+1]$ and $\phi_m=\phi_h=10$. The delayed rectifier $I_K=g_Kn^4(V-V_K)$, where $\alpha_n=-0.01(V+30)/[\exp[-0.1(V+30)]-1]$, $\beta_n=0.125\exp[-(V+40)/80]$ and $\phi_n=15$. Finally, $I_M=g_Mm(V-E_K)$, $m_\infty=1/[1+\exp[-(V+44)/6]]$ and $\tau_m=100/[\exp[-(V+44)/12]+\exp[(V+44)/12]]$.

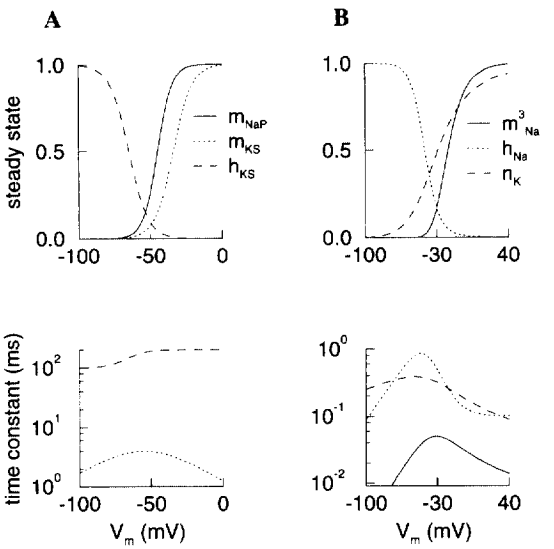

Fig. 2. The kinetic parameters as a function of membrane potential: steady-states (upper panels) and time constants (lower panels). (A) I_{NaP} and I_{KS}. (B) I_{Na} and I_K. Note the window current of I_{Na} around $V=-30$ mV.

Unless specified otherwise, the following parameter values are used: $g_L=0.05$, $g_{Na}=45$, $g_K=18$, $g_{NaP}=0.14$, $g_{KS}=9$, $g_{Ca}=1$, $g_{KCa}=15$, $g_M=0.4$, $g_{input}=0.0$ or 0.012 (in mS/cm^2); $E_L=-50$, $E_{Na}=+55$, $E_K=-90$, $E_{Ca}=+120$, $E_{input}=0$ (in mV). The resting state (with $I_{app}=0$ and $g_{input}=0$) is at -64 mV.

The voltage-dependent steady-states and time constants of I_{Na}, I_K, I_{NaP} and I_{KS} are plotted in Fig. 2. Note that there is a window current of the inactivating I_{Na}, located in a more depolarized voltage range than the half-activation of I_{NaP}. Although g_{NaP} is much smaller than g_{Na} ($g_{NaP}/g_{Na}=0.3\%$), in total current (nA) the I_{NaP} is about 18 times larger than the steady-state I_{Na} at -60 mV, and is always more than four times larger in the subthreshold voltage range ($V<-50$ mV).

Stochastic synapse model with short-term plasticity

The chattering cell model was considered as presynaptic to a fast spiking interneuron model. The latter was taken directly from Ref. 63, where it was constructed so that the model compares well with the characteristics of fast spiking cells, such as the amplitude of spike after hyperpolarization and the frequency–current relation. The chattering cell-to-interneuron synaptic current $I_{syn}=g_{syn}s(V-V_{syn})$, where $g_{syn}=0.05$ mS/cm^2 and $V_{syn}=0$ mV. The channel gating variable s obeys first-order kinetics,[64] $ds/dt=k_fF(V_{pre})\xi(t)(1-s)-k_rs$, with $k_f=12$ and $k_r=1/\tau_{syn}=1$ /ms, $F(V)=1/[1+\exp(-V/2)]$. Given a presynaptic spike, $\xi(t)=1$ if there is vesicle release and 0 otherwise.

The stochastic model of synaptic release (Fig. 1B) is endowed with short-term facilitation[6,56,68] and depression.[1,32,53] The synaptic terminal is assumed to have a number N of available vesicles at any time (N is smaller than a maximum N_0); upon arrival of an action potential, each vesicle can be released with a certain probability p_v, but there is no more than one vesicle release.[49] The spike-triggered release probability is $p=1-e^{-p_vN}$ (see Ref. 6). When a release occurs N is reduced by 1; between spikes the N_0-N vesicles are refilled back to the available pool by a Poisson process with time constant τ_D. The number of immediately available vesicles N_0 has been directly measured at single synapses of hippocampal pyramidal neurons, typically ranging from a few to two dozen.[8,50] We used $N_0=20$. The refill of releasable vesicle pool has a time constant of a few seconds.[50] However, there are faster processes such as a refractory period of tens of milliseconds following vesicle release.[49,54] This is likely related to the observation that short-term synaptic depression exhibits several time constants.[61] We chose $\tau_D=300$ ms, intermediate between the fast recovery from a refractory period and the slow refill process.

In the limit where N_0P_v is sufficiently small, the average behavior of our stochastic model is identical to the existing phenomenological, deterministic models for short-term synaptic depression.[1,25,59] Consider, for example, a repetitive train of presynaptic stimuli at frequency $r=1/\Delta t$. For small N_0P_v, we can approximately write

$$p=1-e^{-p_vN}\simeq 1-(1-p_vN)=p_vN,$$

so p is linear in N. Let $p(k\Delta t)=p_vN(k\Delta t)$ denote the release probability at the kth spike, averaged over trials. Since there is zero or one vesicle release with probability $[1-p(k\Delta t)]$ and $p(k\Delta t)$, respectively, the number of available vesicles immediately after the kth spike is $N'(k\Delta t)=N(k\Delta t)-p(k\Delta t)=N(k\Delta t)(1-p_v)$. The number of unavailable vesicles is $N_0-N'(k\Delta t)$. Between the kth and $(k+1)$th spikes, the unavailable vesicles recover back to the available pool with time constant τ_D, so that upon arrival of the $(k+1)$th spike, the number of unavailable vesicles is $[N_0-N'(k\Delta t)]\exp(-\Delta t/\tau_D)$. Therefore, the number of available vesicles is

$$N[(k+1)\Delta t]=N_0-[N_0-N'(k\Delta t)]\exp(-\Delta t/\tau_D)=N_0[1-\exp(-\Delta t/\tau_D)]+N(k\Delta t)(1-p_v)\exp(-\Delta t/\tau_D),$$

which gives $N[(k+1)\Delta t]$ as a function of $N(k\Delta t)$. Solving this iteration, we obtain

$$p(k\Delta t)=p_{ss}+(p_{init}-p_{ss})\exp(-k\Delta t/\tau_D^*),$$

where $p_{init}=p_vN_0$. The characteristic time constant τ_D^* is given by

$$\frac{1}{\tau_D^*}=\frac{1}{\tau_D}+r\ln\frac{1}{1-p_v}.$$

This implies that, in general, τ^*_D is much shorter than the recovery time constant τ_D. For example, if $r=20$ Hz, and $p_v=0.4$, then $\tau^*_D=73.8$ ms with $\tau_D=300$ ms, and $\tau^*_D=94.8$ ms with $\tau_D=3000$ ms.

The steady-state p_{ss} is given by

$$p_{ss}=\frac{p_vN_0[1-\exp(-1/r\tau_D)]}{1-(1-p_v)\exp(-1/r\tau_D)},$$

which is the same as that of previous phenomenological models.[1] In particular, at high frequencies, $p_{ss}\sim N_0/r\tau_D$, which is inversely proportional to the stimulus rate and independent of p_v.[1,59]

For an arbitary presynaptic train of spikes at times $[t_1, t_2, \ldots]$, the dynamics of $D(t)=p(t)/p_0=N(t)/N_0$ is captured by the following differential equation:

$$\frac{dD}{dt}=-\ln\left(\frac{1}{1-p_v}\right)\sum_j\delta(t-t_j)D+(1-D)/\tau_D.$$

We note that the linear approximation is not accurate unless N_0p_v is small. All the stimulation results reported in this paper were obtained using the original non-linear formula $p=1-e^{-p_vN}$.

Short-term facilitation is due to spike-triggered calcium processes and generally shows several components with

different time constants.[68] Here, we only included one time constant, and facilitation was modeled as $p_v = p_0 F^4$. The dynamics of F is adopted from Ref. 3 (reformulated for spikes as point events in time): F is updated to $1+\alpha_F(F-1)$ upon arrival of a presynaptic spike, and it decays back towards zero between spikes with a time constant τ_F. F, then p_v, is evaluated after the spike. The dynamics of $F(t)$ thus described obeys the following equation:

$$\frac{dF}{dt} = \ln\left(\frac{1}{\alpha_F}\right)\sum_j \delta(t-t_j)(1-F) - F/\tau_F$$

Note that the parameter α_F controls the facilitation potency: one can show that, in response to two stimuli separated by a small time interval, $F_1 = 1-\alpha_F$, whereas the paired-pulse facilitation $F_2/F_1 = 1+\alpha_F$ (cf. Ref. 3).

When simulated by sustained presynaptic spike discharges, our dynamical synapse model shows strong facilitation if the initial release probability is low and N_0 is not too small; otherwise, short-term depression due to vesicle depletion dominates. A detailed model analysis will be presented elsewhere (Matveev V. and Wang X.-J., unpublished observations). In order to mimic strong facilitation as commonly reported for local pyramid-to-interneuron connections in the neocortex, we chose $p_0 = 0.05$, $\alpha_F = 0.55$ and $\tau_F = 100$ ms. See Results (Fig. 8) for comparison with experimental data.

In stimulations, we somewhat arbitrarily used three synaptic contacts between the cell pair, so that the postsynaptic cell can be driven to fire action potentials, but a single release is usually not sufficient to trigger a spike. Examples from the hippocampus have been documented where a single pyramidal cell is capable of eliciting discharges in a connected postsynaptic interneuron.[34]

Numerical methods

The model was stimulated on a Silicon Graphics Workstation, using a fourth-order Runge–Kutta method ($dt = 0.02$ ms). Power spectra were computed using the subroutine *spctrm.c* from *Numerical Recipes*,[40] modified by Yinghui Liu.

RESULTS

Ping-pong mechanism for rhythmic bursting

When stimulated by a current pulse, the neuron model displays rhythmic burst firing of spikes similar to the observed behaviors of chattering cells (Fig. 3A). Common characteristics include the following. (1) Each burst typically terminates with a significant afterdepolarization (ADP) and is followed by a slower afterhyperpolarization (Figs 3, 4A). (2) Action potentials are fast in duration (0.3 ms at half-amplitude), primarily due to rapid gating kinetics of the I_K. (3) At sufficiently large current intensity, the firing becomes tonic at high frequencies (Fig. 4A). Such a transition has been reported in Ref. 46 (reproduced in Fig. 5), which came to our attention after the present paper was submitted for publication. (4) The burst frequency is low for a restricted range of small I_{app} values, but typically is about 20–40 Hz. The current range for rhythmic bursting is comparable with the experimental measurements (Fig. 4B, upper panel). (5) With increased applied current intensity, the intra-burst firing frequency is about 300–500 Hz (Fig. 4B, middle panel) and the number of spikes per burst increases stepwise (Fig. 4B, lower panel).

Repetitive bursting is primarily generated by a "ping-pong" interplay between action potentials in the somatic compartment and slow active currents in the dendritic compartment.[39,41,57,58] As illustrated in Fig. 3B, when the somatic membrane potential V_s fires an action potential, the dendritic V_d is depolarized gradually in time, because the electrotonic coupling between the two compartments is relatively weak, and the dendrite has a much larger capacitance than the soma. As V_s repolarizes, the V_d depolarization lingers and is boosted by the activation of the inward I_{NaP}. This then feeds back an inward current flow to the V_s and elicits another somatic spike. This ping-pong process repeats itself until the outward I_{KS} is sufficiently activated to repolarize the cell, so that the soma finally fails to reach the firing threshold. Thus, the burst terminates with a subthreshold ADP. During the inter-burst afterhyperpolarization the I_{KS} decreases, the cell recovers to its initial state and the burst starts anew.

The ADP has several (passive and active) components originating from both the dendrite and soma. Note that the dendrite-to-soma current flow is inward and depolarizing (when $V_d > V_s$) only during a brief time (less than 1 ms) at the repolarization of somatic spikes (Fig. 3B). The ADP begins within this time window but develops fully only afterwards (when $V_d < V_s$; hence, the dendrite-to-soma current is outward). Therefore, the I_{Na}, the only somatic inward current which is significant near the firing threshold, must have taken over and contributed to the generation of the ADP. In order to test whether the initial dendrite-to-soma inward current is necessary at all for the ADP, we artificially clamped V_d to be more hyerpolarized than V_s by 2 mV only during the brief time when normally V_d would have been more depolarized than V_s. When such manipulation was done after the third spike in Fig. 3B, the ADP was completely abolished. When it was done after the second spike, the burst was terminated immediately without the third spike or an ADP (data not shown). Therefore, the ADP generation in our model requires an initial dendrite-to-soma depolarization followed by an activation of the somatic window I_{Na} (which is smaller and has a higher voltage threshold than I_{NaP}).

In our model, the ADP and rhythmic bursting do not depend critically on the high-threshold Ca^{2+} conductance g_{Ca}. As shown in Fig. 6A, with $g_{Ca} = 0$ (hence I_{KCa} is zero as well), the chattering pattern remains the same as before (compare with the voltage trace with $I_{app} = 0.65$ nA in Fig. 4A). The burst frequency is slightly increased (44 Hz vs 41 Hz), which can be explained by the blockade of I_{KCa}. Indeed, the main effect of g_{Ca} is its activation of I_{KCa}, which is important to stabilize the membrane. Without dendritic I_{KCa}, the powerful g_{NaP} could lead to

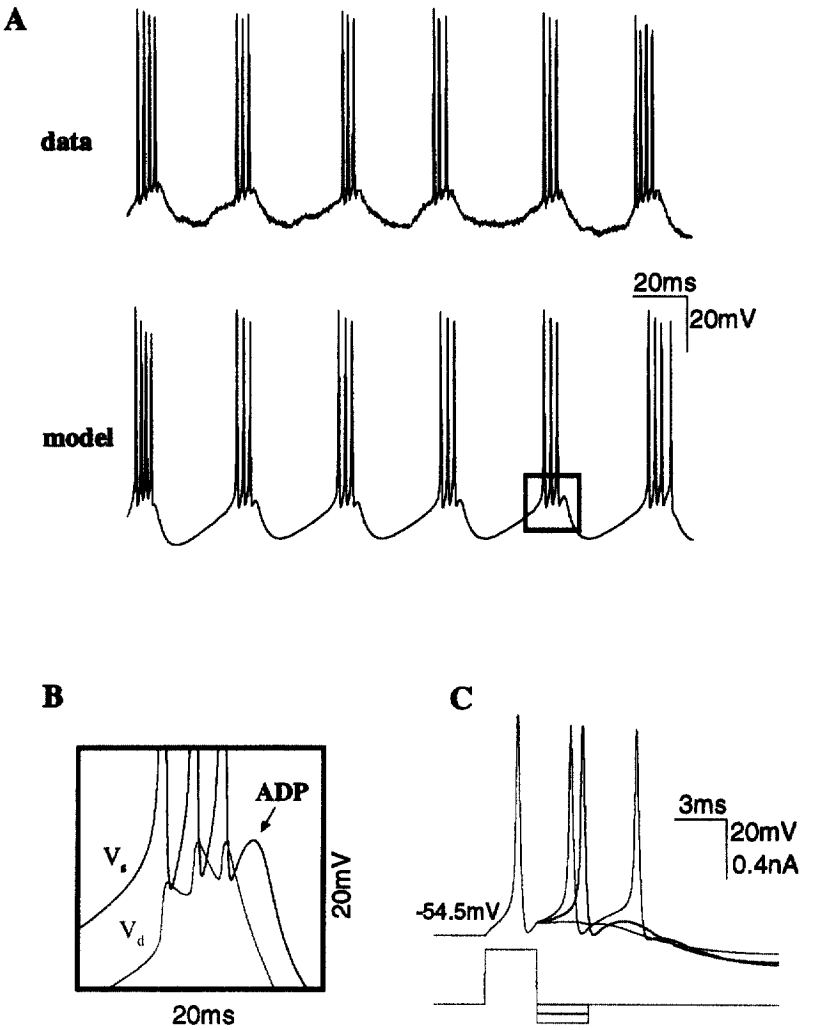

Fig. 3. Behavior of model neuron. (A) Comparison between an *in vivo* intracellular voltage trace from the cat visual cortex (courtesy of McCormick D. A. and Gray C. M.) and model simulation. This particular cell has a relatively low frequency among recorded chattering cells. In order to better match with this example, we slowed down the I_{KS} (with τ_0=25 ms), and varied slightly g_{NaP} (=0.1) and g_K (=14). The injected current intensities are 0.61 and 0.58 nA for the data and the model, respectively. (B) An enlarged burst from the lower panel in A with superimposed somatic and dendritic membrane potentials. Note the pronounced spike ADP. (C) Slow membrane depolarization underlying a burst can be unmasked by applying a hyperpolarizing pulse immediately after a threshold-straddling current pulse. Using hyperpolarizing pulses of different amplitudes (in blue and red), the third or second spike is abolished, and the unmasked depolarizing wave lasts for about the duration of the burst.

unrealistic runaway excitation of the cell, especially when the cell is stimulated by strong inputs to the dendritic compartment (data not shown).

Interestingly, when both g_{NaP} and g_{Ca} were blocked, the dendrite became completely passive, we still observed ADP and doublets of spikes (Fig. 6B). However, the corresponding range of injected current intensities is much more restricted (0.62–0.77 nA), compared with 0.3–1.0 nA of Fig. 4. In this case, the ADP is largely produced by the somatic Na^+ window current, but is initially triggered by a passive charge redistribution from the large dendritic capacitance to the soma.[51] Hence, even when the dendrite is passive, the ADP may be sufficient to produce doublets of spikes, but not bursts of spikes in a robust way.

Cholinergic modulation

Although the two other K^+ conductances g_M and g_{KCa} are not essential for rhythmogenesis itself, they can greatly alter the bursting dynamics. As mentioned before, I_{KCa} controls the excitability of the dendritic membrane. On the other hand, I_M, being of low activation threshold and located in the somatic compartment, was found to be very effective in limiting the number of spikes per burst. This is shown

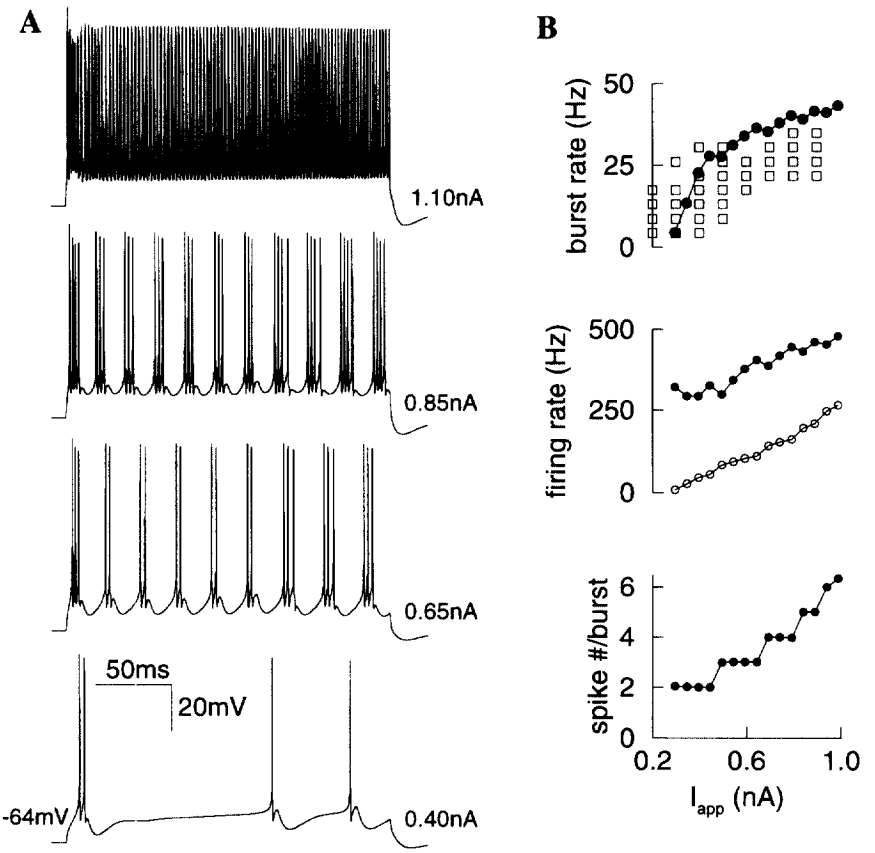

Fig. 4. (A) Fast rhythmic bursting elicited by injected current pulses (intensity shown near the traces). At large I_{app}, the firing pattern becomes tonic with firing frequencies larger than 350 Hz (top panel). (B) Upper panel: bursting frequency as a function of I_{app}. The open squares are data from an intracellularly recorded chattering cell (courtesy of McCormick D. A. and Gray C. M.). Middle panel: intra-burst firing frequency and mean firing frequency (filled and open circles, respectively). Lower panel: number of spikes per burst as a function of I_{app}.

in Fig. 7, where the cholinergic modulation of these two channels is simulated.[30] Initially, the g_M and g_{KCa} are set to be sufficiently large so that the cell fires only single spikes, each followed by a noticeable ADP. The tonic firing is transformed into burst firing when g_{KCa} and especially g_M are reduced by simulated cholinergic action (Fig. 7). This result is consistent with recent *in vitro* observations,[33] and suggests that the g_M and g_{KCa} are likely targets of cholinergic modulation for the pacemaker behavior of chattering cells.

Reliable pacemaker across unreliable synapses

At present, the short-term plasticity properties of the synaptic connections made by chattering neurons remain unknown. We considered a hypothetical connection from a chattering cell to a fast spiking inhibitory interneuron. As explained in the Computational Procedures, the stochastic synapse model behaves similarly to the pyramid-to-interneuron connections found by Thomson *et al.*,[56] with a low initial release probability and strong short-term facilitation. An example of the synapse model behavior is shown in Fig. 8A, with repetitive presynaptic stimulation at 30 Hz. The individual postsynaptic responses display frequent transmission failures, and the trial-averaged response exhibits pronounced facilitation comparable with the experimental measurements of Thomson and Deuchars (Fig. 8B). For the parameter set specified in the Computational Procedures, the initial release probability is $p=0.04$, so that the probability of transmission failure is $(1-p)^3=88\%$ (with three synaptic contacts). By comparison, the failure probability is reported to be >80% for a reconstructed local pyramid-to-interneuron connection with three synaptic contacts.[55]

This synapse model is used for a chattering cell to drive an interneuron. The chattering cell is now excited by Poisson synaptic inputs instead of current pulses, so that its firing patterns are somewhat noisy (Fig. 9A, top panel). Because of a low p, there are frequent failures of synaptic transmission (Fig. 9A, second panel), and the postsynaptic cell fires an action potential when there are multiple release events during a presynaptic burst (Fig. 9A, third and

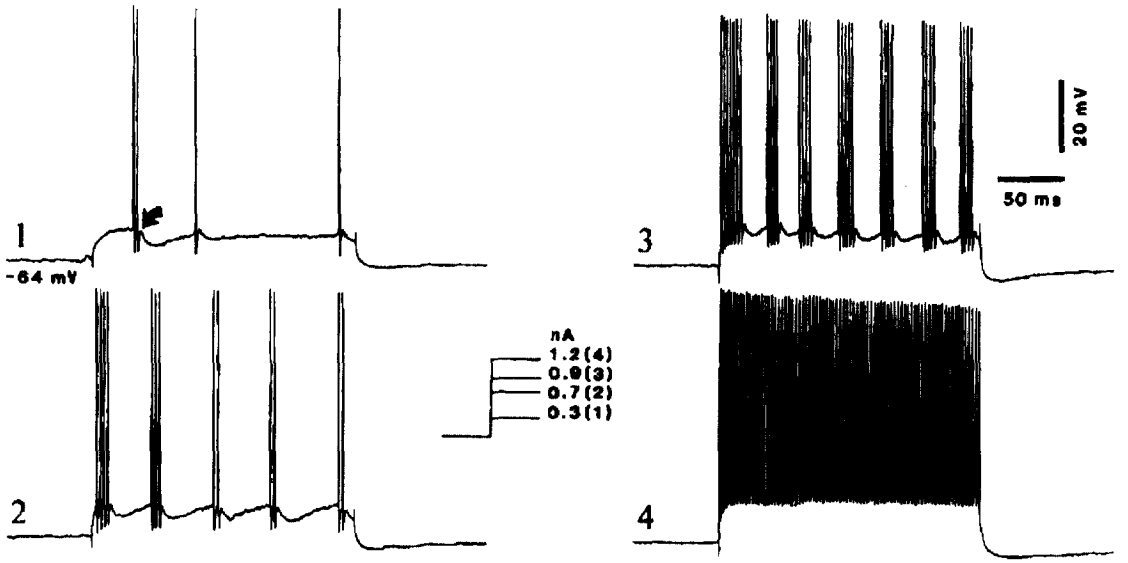

Fig. 5. Chattering behavior of a corticothalamic pyramidal neuron in the cat association neocortex (reproduced from Ref. 46 with permission). Membrane potentials with four injected current intensities are shown. Note the similarity with Fig. 4A.

fourth panels). A large fraction (60%) of chattering cell interspike intervals are very short (<3 ms), belonging to rapid bursts (Fig. 9B). By contrast, the inter-release interval histogram (IRIH) of the synapses is characterized by multiple peaks and a long tail (Fig. 9B). Only less than 20% of the inter-release intervals are smaller than 3 ms (Fig. 9B) because, with a low p, it is relatively rare that there are several releases at a single synaptic site during a presynaptic burst. The interspike interval histogram (ISIH) for the chattering cell displays a characteristic bimodality, while the ISIH of the postsynaptic cell does not show an obvious rhythmicity (Fig. 9C).

In order to assess the importance of bursts, we compared the tonic firing with rhythmic bursting of the presynaptic cell, with the same steady-state release probability p (Fig. 10A–C). Here, the postsynaptic interneuron is hyperpolarized to -75 mV in order to delineate the excitatory postsynaptic potentials (EPSPs). In the bursting mode (Fig. 10A, red curve), although the ISIH of the interneuronal spike discharges does not show rhythmicity (Fig. 9C), the membrane fluctuations are rhythmic, as evidenced by a pronounced peak (at $f_{max} \simeq 45$ Hz) in the power spectrum of EPSPs (Fig. 10B, red curve). This power spectrum was computed averaged over trials; thus, the rhythmicity is robust in spite of considerable variability in the presynaptic firing pattern that differs from trial to trial (the coefficient of variability of interspike intervals is 0.95 in the rhythmic bursting case). By contrast, in tonic firing mode (Fig. 10A, blue curve), as a result of transmission failures the input to the interneuron often skips cycles of the presynaptic rhythm, so that the power spectrum of the EPSPs no longer shows rhythmicity (Fig. 10B, blue curve).

We emphasize that as far as the rhythmicity is concerned, the above result cannot be explained simply by the fact that the presynaptic firing rate is higher in the burst mode than in the tonic mode. To illustrate the point, we repeated the simulation with $g_{NaP}=0$, when the chattering cell model no longer shows rhythmic bursting but preserves the same firing rate (about 120 Hz) as before (by adjusting the Poisson input rate) (Fig. 10A, green curve). As expected, in this case the rhythmicity is completely absent in the postsynaptic power spectrum (Fig. 10B, green curve).

The rhythm transmittability is further quantified in Fig. 10C, where one sees that, in the bursting mode, the postsynaptic ryhthmicity is still significant even if $p<0.1$. By contrast, in the tonic firing mode, the postsynaptic rhythmicity is not discriminable even with $p \simeq 0.4$. Therefore, burst firing is a dramatically more robust mode for pacing the rhythm across unreliable cortical synapses.

In addition to the steady-state behaviors, interesting transient dynamics were observed due to the short-term synaptic plasticity. Indeed, bursting is more effective than tonic firing in inducing synaptic facilitation (by $[Ca^{2+}]_i$ accumulation at the synaptic terminal; Fig. 10D, upper panel), but it also leads to more transmitter release and hence synaptic depression (Fig. 10D, middle panel). Therefore, in the bursting mode, the release probability p first increases rapidly due to facilitation, until vesicle depletion takes over and p decreases to a steady state (Fig. 10D, lower panel). By contrast, in the tonic firing mode, the time-course of facilitation (hence p) lacks a fast rising phase and is more gradual, thus there is a relatively long time window (about 250 ms), during which the release probability per spike is significantly

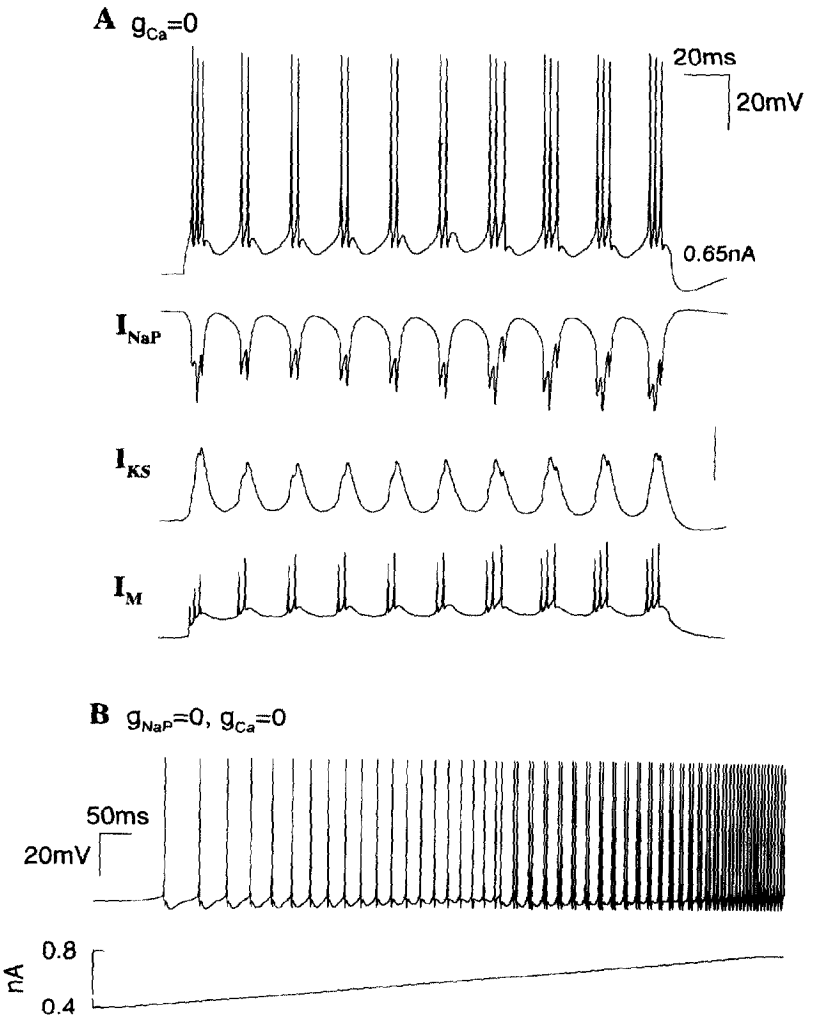

Fig. 6. Blockade of active conductances in the dendrite. (A) With $g_{Ca}=0$ ($I_{app}=0.65$ nA), the chattering pattern remains similar to the control case (cf. Fig. 4A), but the burst frequency is slightly higher because of the blockade of I_{KCa} as a consequence. Also plotted are all other active currents, with the vertical bar corresponding to 2.5, 5 and 15 A/cm^2 for I_{NaP}, I_{KS} and I_M, respectively. (B) Blocking both g_{NaP} and g_{Ca} does not completely abolish the rhythmic burst firing, as shown by a slow ramp of I_{app}.

higher in the bursting mode than in the tonic firing mode (Fig. 10D, lower panel).

Recruitment of inhibitory interneurons

This last observation is interesting, given that, in behaving conditions of the brain, visual inputs are usually not constant in time, so a steady state may never be realized. This is illustrated in Fig. 11, where a sinusoidal input is applied to the chattering cell at 3 Hz, which mimics a visual moving grating stimulus. The postsynaptic interneuron is shown to fire vigorously when driven by presynaptic bursts of discharges, whereas it rarely reaches spike threshold when the presynaptic cell is switched to the tonic firing mode. In this case, because the presynaptic spike output is not constant in time, the synaptic release probability p never reaches a steady state. Instead, p increases more steeply in time and remains significantly higher all the time, in the bursting mode than in the tonic mode (Fig. 11). Therefore, rapid bursting is effective in recruiting its postsynaptic targets, not only because of its high firing rate, but also because of an enhanced probability per spike for the synaptic transmission.

DISCUSSION

We have presented an ionic conductance model, and explored some possible functional implications, of the fast ($\sim$40 Hz) rhythmic bursting of chattering neurons in the neocortex. In our model, the oscillation mechanism is similar to that in Ref. 62, but here the rhythm-generating currents I_{KS} and I_{NaP} are assumed to be located at dendritic sites sufficiently isolated from the soma. The rhythmogenesis depends on three important cellular properties. First, a pronounced ADP, which in our model has three

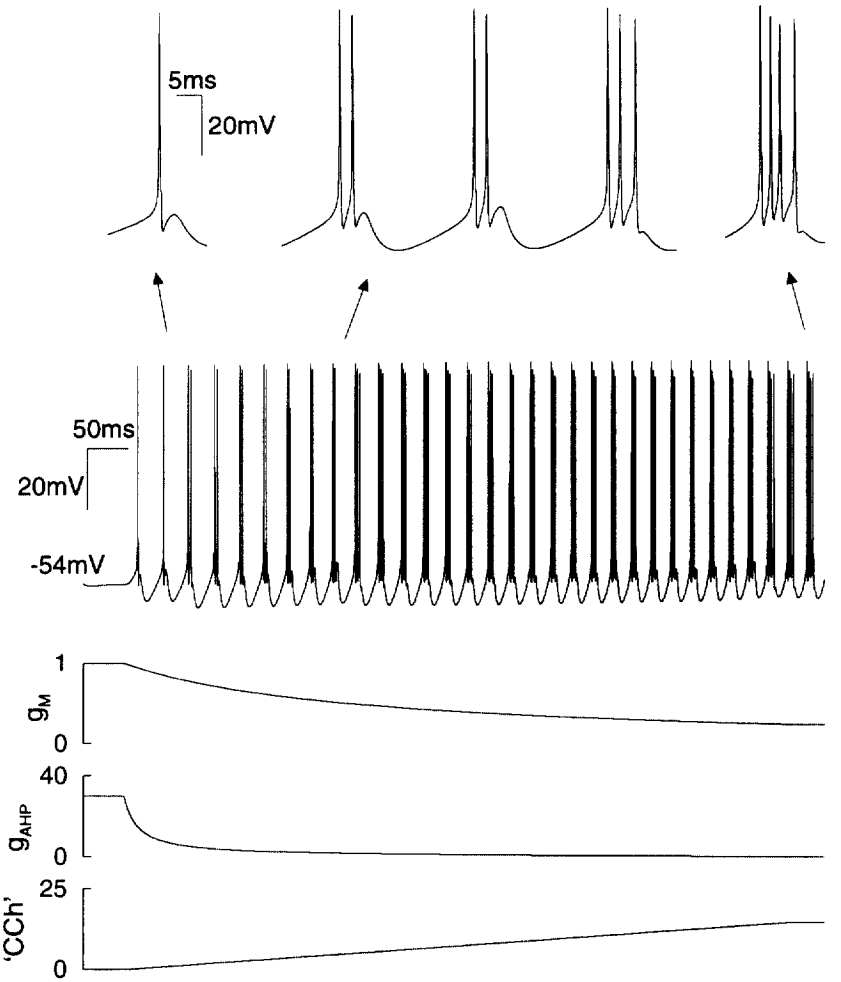

Fig. 7. Simulated modulation of burst firing by acetylcholine. Both g_M and g_{KCa} are assumed to be reduced by an agonist (carbachol, CCh) of muscarinic acetylcholine receptors, according to the expression $g=g_0 IC_{50}/(CCh+IC_{50})$, with $IC_{50}=0.3$ μM for g_{KCa} and 5 μM for g_M.[30] The model neuron is transformed from firing tonically (with spike ADP) to bursting rhythmically as g_M and g_{KCa} are gradually reduced by a ramp of carbachol pulse. The transformation is in parallel with the time-course of the g_M decrease. Inserts at the top illustrate enlarged single spike and bursts at three different levels of modulation ($I_{app}=0.55$ nA).

components. It is generated by an initial dendrite-to-soma inward current flow due to both the activation of the dendritic I_{NaP} and a passive charge redistribution, followed by the activation of the somatic Na^+ window current. Second, weak coupling between the soma and dendrites with a large capacitance provides a suitable neuronal electrical structure for the "ping-pong" interplay between action potentials and the dendrite-dependent ADP. Finally, a slow K^+ current is the primary determinant of the burst duration and the inter-burst afterhyperpolarization (hence the oscillation period).

Other models of pyramidal bursters[39,41,57,58] share similar qualitative requirements for the burst firing behavior, but are based on Ca^{2+} rather than Na^+ currents and have much slower rhythmic frequencies. Note that our model would work as well if the persistent dendritic Na^+ current was substituted by an inactivating Na^+ current, provided that the latter displayed a window current of sufficiently low voltage threshold and large amplitude.[5] Sodium currents have been demonstrated in dendrites of cortical pyramidal cells, including a persistent Na^+ component.[35,43,52] Moreover, an I_{Na}-dependent burst firing pattern has been reported in pyramidal neurons,[9,20] but none of them display such fast rhythmicity as the chattering cells. In addition to the I_{NaP}, our rhythmogenesis mechanism depends on a voltage-gated K^+ ion channel, which is presumably a slow subtype of the A-type-inactivating K^+ channels. Little is known about dendritic K^+ channels in neocortical pyramidal cells, but a recent study revealed a surprisingly high density of transient A-type K^+ channels in dendrites of hippocampal pyramidal neurons.[17] It seems unlikely that fast gamma oscillations could be generated by a K^+ current that depends on spike-triggered

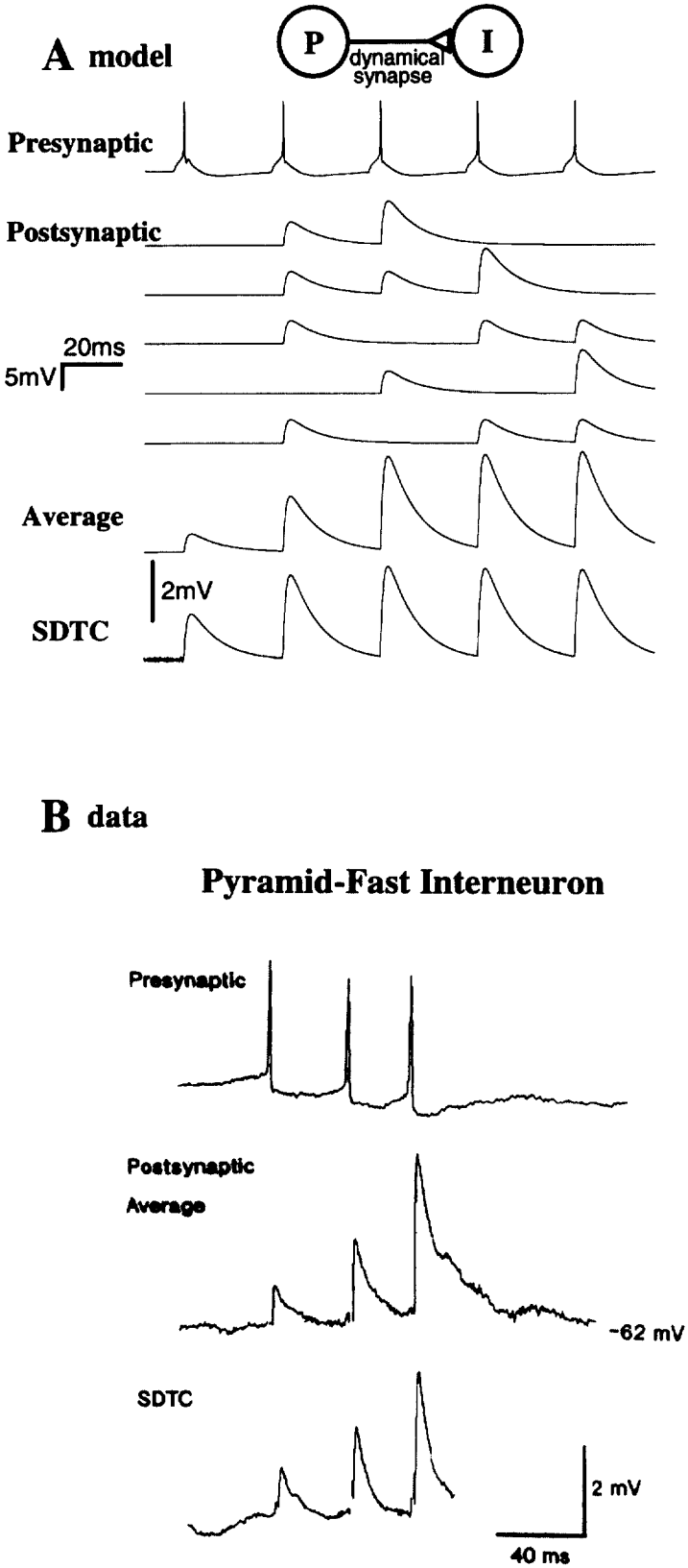

Fig. 8. (A) Short-term facilitation of the synapse model (with three synaptic contacts), in response to a train of repetitive presynaptic firing at 30 Hz. Frequent transmission failures are evident in the five samples of the postsynaptic response. The average response was obtained with 100 samples. SDTC is the standard deviation time-course; its large value indicates a high trial-to-trial variability of the postsynaptic response (g_{syn}=0.1). (B) An example of postsynaptic response recorded from a pyramid-to-fast interneuron connection of the rat somatomotor cortex (reproduced from Ref. 54 with permission). The model behavior in A displays strong facilitation, similar to the experimental data in B.

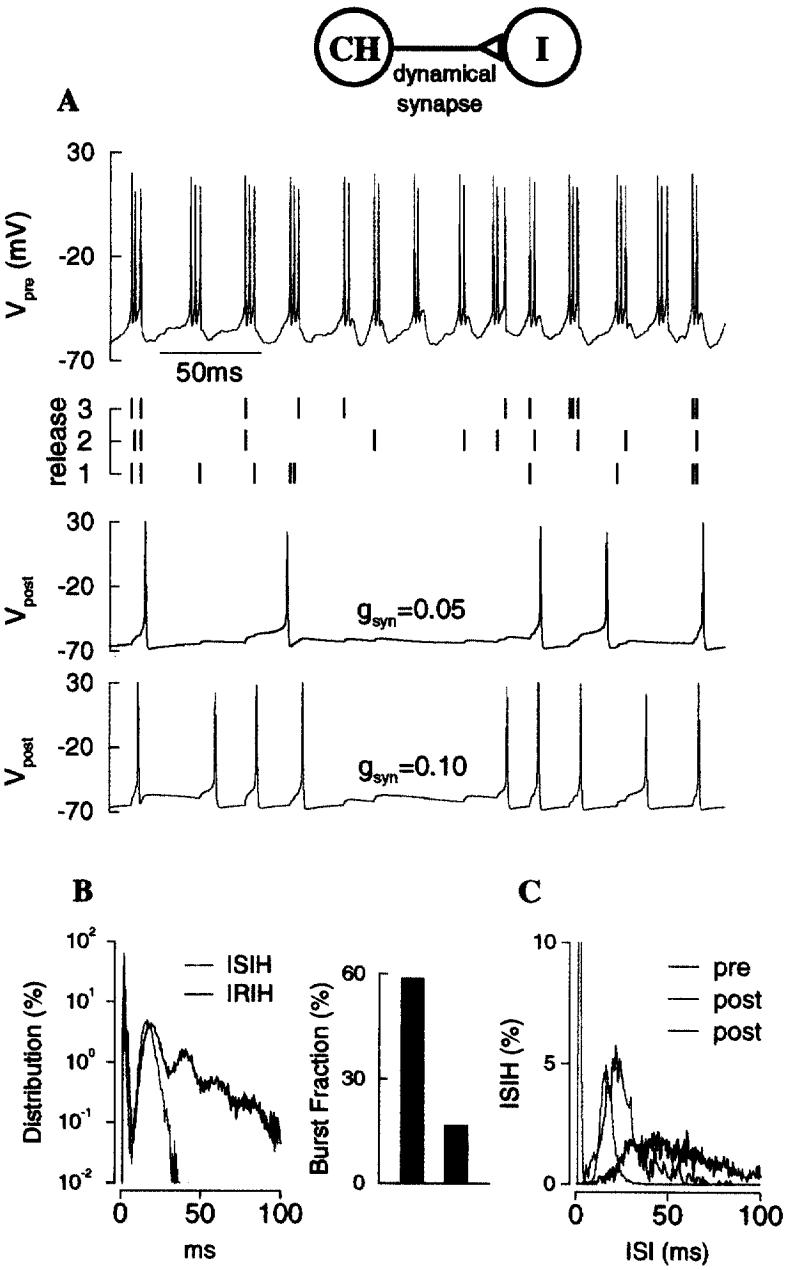

Fig. 9. Chattering cell synaptically drives a postsynaptic interneuron. (A) The chattering neuron fires bursts of spikes in response to Poisson inputs (top panel). There are numerous transmission failures at the three release sites (second panel), and the postsynaptic cell typically fires a spike when there are multiple releases during a presynaptic burst (third and fourth panels). The postsynaptic firing rate is about 16 Hz with $g_{syn}=0.05$ and 34 Hz with $g_{syn}=0.10$. (B) Left panel: compared to the ISIH of the presynaptic cell (red), the IRIH of the synapses (black) shows several maxima and a long tail, reflecting transmission failures at consecutive presynaptic bursts. Right panel: the burst fraction (time interval <3 ms) is 59% for the ISIH and 17% for the IRIH. (C) The ISIH of the chattering cell is bimodal (red), whereas that of the postsynaptic cell is wide and unimodal (blue and green). $g_M=0.3$, $\lambda=3$ kHz.

calcium influx (such as the calcium- and voltage-dependent I_C). This is because calcium accumulation and decay are typically too slow compared to the chattering burst duration ($\sim$5 ms) and oscillation period ($\sim$20 ms), respectively; chattering cells fire thin spikes, hence calcium influx per spike is expected to be small. Obviously, further experimental and modeling investigations are needed in order to test this theoretically proposed mechanism.

Pyramidal cells in the electrosensory lateral-line lobe of weakly electric fish display short bursts of spikes that depend on dendritic Na^+ channels,[60] and this burst firing has been implicated in the extraction of special temporal features from stimulus.[12] In

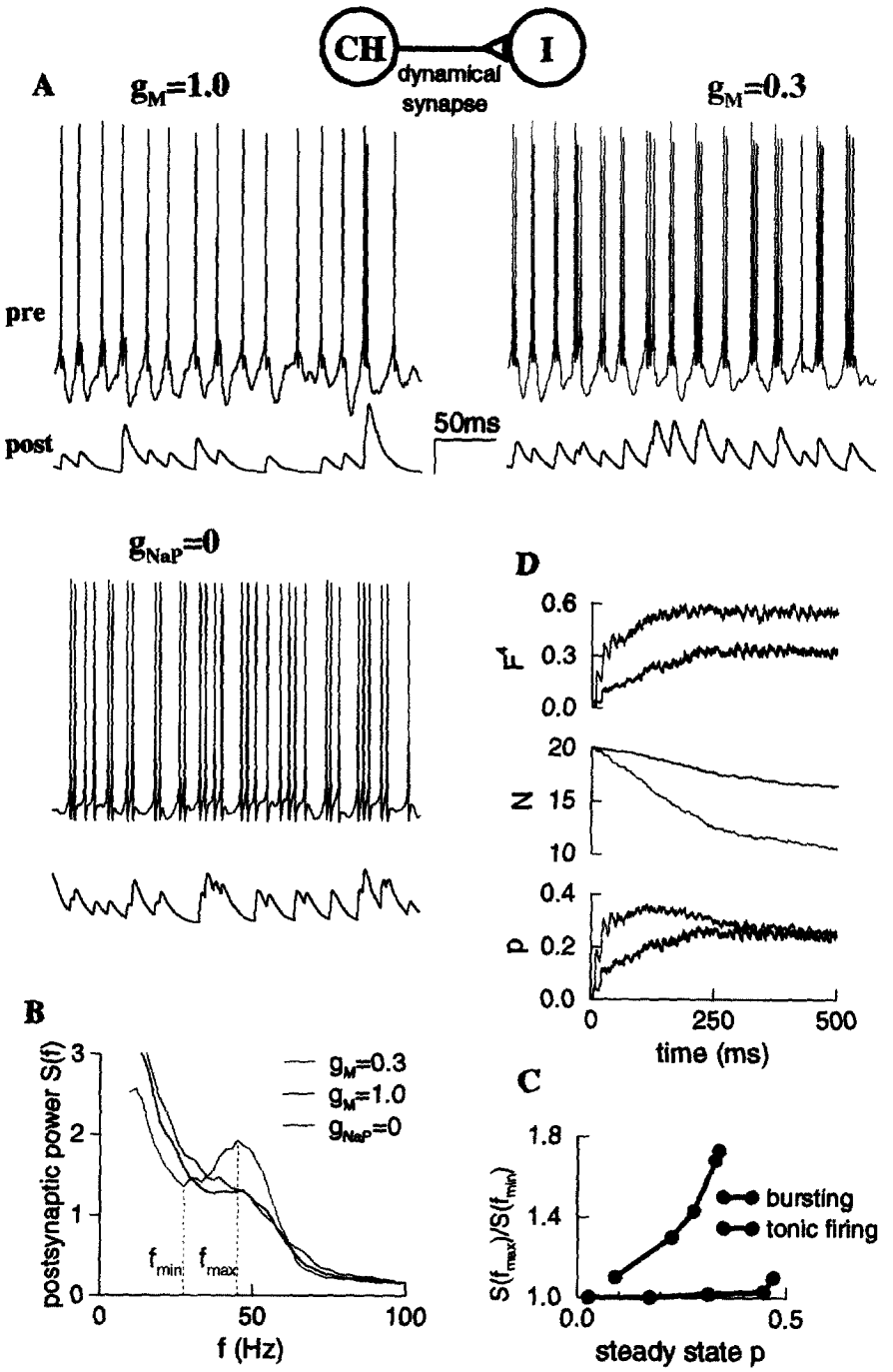

Fig. 10. Transmission of gamma rhythmicity across stochastic synapses. (A) With a large g_M, the chattering cell fires tonically, and the postsynaptic cell (hyperpolarized to $V_{rest}=-75$ mV) frequently skips cycles due to transmission failure (blue). By contrast, with reduced g_M, presynaptic burst firing leads to more reliable transmission per cycle, hence the rhythmicity is preserved in the postsynaptic cell (red). The firing pattern with $g_{NaP}=0$ (green) has a similar firing rate as the rhythmic bursting case. The voltage bar is 10 mV (respectively 5 mV) for the pre- (respectively post-) synaptic cell. (B) Power spectrum of postsynaptic potential computed by averaging over 20 trials. The red curve (but not the blue and green ones) displays a clear peak at about 45 Hz. As in A, time traces were obtained after a transient of 500 ms. The high power at low frequencies is due to temporal correlations caused by the short-term synaptic plasticity (cf. the IRIH in Fig. 9C), and was absent if a deterministic synapse model was used (data not shown). The postsynaptic rhythmicity is quantified as the ratio between the power at the peak frequency (f_{max}) to that at the trough frequency (f_{min}). The larger this ratio is above 1, the more prominent is the postsynaptic oscillation. This ratio is plotted in C as a function of the steady-state p, which was varied by changing the facilitation parameter α_F from 0.1 to 0.9. The ratio is always close to 1 in the tonic firing mode, whereas it remains significantly larger than 1 in the bursting mode, even for very low p. (D) Transient time-courses of synaptic facilitation F^4, the number of available presynaptic vesicles N and the release probability $p=1-e^{-p_0F_4N}$, computed by averaging over 20 trials (input onset at $t=0$). Blue: $g_M=1$ and Poisson input rate $\lambda=4$ kHz; red: $g_M=0.3$ and $\lambda=3$ kHz ($g_{input}=0.012$ for both blue and red); green: $g_{NaP}=0$, $g_M=0.3$, $\lambda=19$ kHz and $g_{input}=0.0024$.

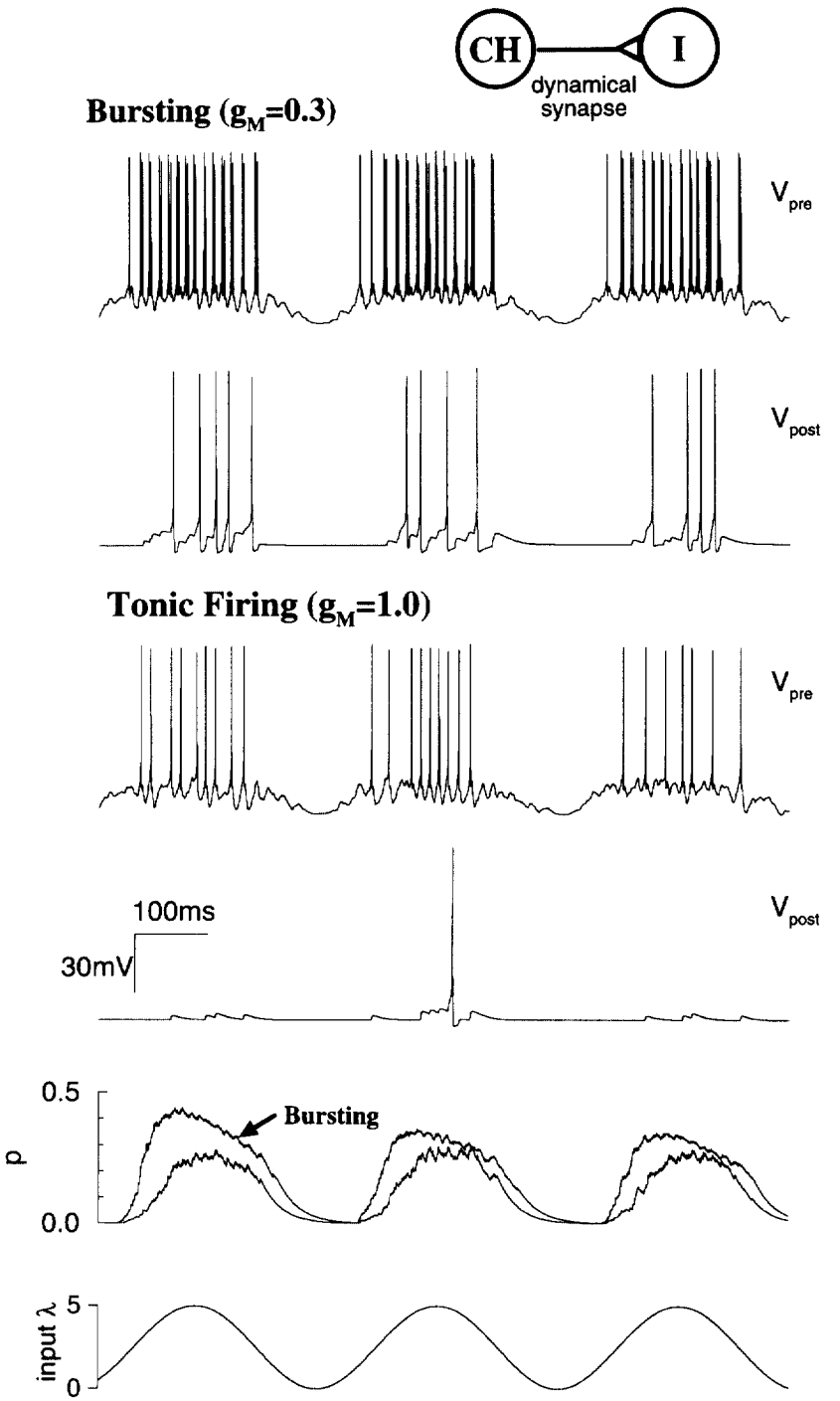

Fig. 11. Recruitment of inhibitory neurons by fast burst firing. In response to a sinusoidal input at 3 Hz (bottom panel, Poisson input rate), fast burst firing of a chattering cell can powerfully excite the postsynaptic cell to fire at relatively high rate, whereas tonic firing fails to generate significant postsynaptic discharges. The release probability per spike (p) is much higher in the bursting than in the tonic firing mode.

mammalian neocortex, whether fast bursting neurons are assigned some specialized computational functions remains unknown. Previous work on the hippocampus suggested that burst discharges may be effective in inducing long-term synaptic potentiation.[18,23] Recently, Lisman[26] argued that bursts may represent a reliable neural signal across noisy and facilitating synapses. Here, we considered a specific example and investigated a hypothetical case of connections from a chattering cell to a postsynaptic

inhibitory neuron, with a synaptic model that behaves similarly to some pyramid-to-interneuron connections.[56] When the chattering cell model was driven by a non-stationary input (mimicking a visual moving grating stimulus), the postsynaptic interneuron could be effectively recruited to fire spikes by presynaptic burst firing. To a large extent, this is simply because a much higher presynaptic firing rate in the bursting mode generates larger postsynaptic responses (this, however, would not be the case for strongly depressing synapses), and few excitatory neurons in the neocortex fire at such high frequencies as the chattering cells. In addition, our results showed that bursts of spikes are more powerful, also because the transmission per spike is more reliable due to burst-induced synaptic facilitation. Therefore, chattering cells may be powerful contributors to the recruitment of feedback inhibition, which is believed to play critical roles in many perceptual computations in the neocortex.[36]

One may ask whether chattering neurons coupled by recurrent excitation can synchronize themselves to generate a population rhythm and to drive coherently other neuronal types in the neocortex. Alternatively, subpopulations of inhibitory interneurons may be particularly capable of synchronizing 40-Hz cortical network oscillations, either by cross-talk with pyramidal cells,[10,66,67] or by mutual interactions among themselves.[63–65] In this second scenario, it can be imagined that chattering cells and certain class(es) of inhibitory interneurons could play the complementary roles of pacemaker and synchronizer, respectively, and the reciprocal synaptic interactions between these two cell populations generate the network 40-Hz oscillations. In this regard, as demonstrated here, the burstiness of rhythmic firing may be important for chattering cells to fulfil a pacemaker role in the neocortex, if the synaptic transmission to interneurons is highly unreliable. We have shown that, as far as the rhythmicity is concerned, the synaptic reliability depends on the burst firing pattern, not just an increased firing rate. It would be interesting to investigate experimentally whether chattering neurons do make low-p and facilitating synapses on some classes of interneurons, and whether such activation of feedback inhibition plays an important role in the network gamma frequency oscillation and synchronization. Such a scenario would be in contrast with other situations where burst firing may not be required for pacing the 40-Hz rhythm, if the pyramid-to-interneuron connections are reliable.[66]

Finally, we showed that the burstiness (number of spikes per burst) can be controlled by acetylcholine modulation, which in the model acts via a reduction of I_M and I_{KCa}. Furthermore, activation of presynaptic muscarinic receptors, by inhibiting transmitter release,[59] could help the synapse to filter out randomly occurring single spikes that are mixed with rhythmic bursts in sensory responses of the chattering cells, thus enhancing the robustness of the gamma rhythmicity in the presence of highly noisy background activity. The chattering behavior could also be potentiated by other neuromodulators, such as serotonin, which has been reported to increase a persistent Na^+ conductance in the apical dendrites of neocortical pyramidal neurons.[2] In this way, chattering cells may become true pacemakers only by reticular formation activation, which could thus promote stimulus-induced gamma oscillations in the neocortex[33,37,47] by transforming chattering cells from tonic firing to rhythmic bursting mode.

Acknowledgements—I thank Drs D. A. McCormick and C. M. Gray for sharing their data with me and for valuable discussions, and Drs L. Abbott, C. Koch, J. Lisman, L. Nowak and A. M. Thomson for helpful comments on the manuscript. This work was supported by the Office of Naval Research, the National Institute of Mental Health, the Alfred P. Sloan Foundation and the W. M. Keck Foundation.

REFERENCES

1. Abbott L. F., Varela J. A., Sen K. and Nelson S. B. (1996) Synaptic depression and cortical gain control. *Science* **275,** 220–224.
2. Aghajanian G. K. and Marek G. J. (1997) Serotonin induces excitatory postsynaptic potentials in apical dendrites of neocortical pyramidal cells. *Neuropharmacology* **36,** 589–599.
3. Bertram R., Sherman A. and Stanley E. F. (1996) Single-domain/bound calcium hypothesis of transmitter release and facilitation. *J. Neurophysiol.* **75,** 1919–1931.
4. Calvin W. H. and Sypert G. W. (1976) Fast and slow pyramidal tract neurons: an intracellular analysis of their contrasting repetitive firing properties in the cat. *J. Neurophysiol.* **39,** 420–434.
5. Crill W. E. (1996) Persistent sodium current in mammalian central neurons. *A. Rev. Physiol.* **58,** 349–362.
6. Dobrunz L. E. and Stevens C. F. (1997) Heterogeneity of release probability, facilitation, and depletion at central synapses. *Neuron* **18,** 995–1008.
7. Eckhorn R., Bauer R., Jordan W., Brosch M., Kruse W., Munk M. and Reitboeck H. J. (1988) Coherent oscillations: a mechanism for feature linking in the visual cortex? *Biol. Cybern.* **60,** 121–130.
8. Forti L., Bossi M., Bergamaschi A., Villa A. and Malgaroli A. (1997) Loose-patch recordings of single quanta at individual hippocampal synapses. *Nature* **388,** 874–878.
9. Franceschetti S., Guatteo E., Panzica F., Sancini G., Wanke E. and Avanzini G. (1995) Ionic mechanisms underlying burst firing in pyramidal neurons: intracellular study in rat sensorimotor cortex. *Brain Res.* **696,** 127–139.
10. Freeman W. J. A. (1964) A linear distributed model for prepyriform cortex. *Expl Neurol.* **10,** 525–547.
11. French C. R., Sah P., Buckett K. J. and Gage P. W. (1990) A voltage-dependent persistent sodium current in mammalian hippocampal neurons. *J. gen. Physiol.* **95,** 1149–1157.

12. Gabbiani F., Metzner W., Wessel R. and Koch C. (1996) From stimulus encoding to feature extraction in weakly electric fish. *Nature* **384,** 564–567.
13. Gray C. M. and McCormick D. A. (1996) Chattering cells: superficial pyramidal neurons contributing to the generation of synchronous oscillations in the visual cortex. *Science* **274,** 109–113.
14. Gray C. M. and Singer W. (1989) Stimulus-specific neuronal oscillations in orientation columns of cat visual cortex. *Proc. natn. Acad. Sci. U.S.A.* **86,** 1698–1702.
15. Gray C. M. and Viana Di Prisco G. (1997) Stimulus-dependent neuronal oscillations and local synchronization in striate cortex of the alert cat. *J. Neurosci.* **17,** 3239–3253.
16. Hodgkin A. L. and Huxley A. F. (1952) A quantitative description of membrane current and its application to conduction and excitation in nerve. *J. Physiol.* **117,** 500–544.
17. Hoffman D. A., Magee J. C., Colbert C. M. and Johnston D. (1997) K^+ channel regulation of signal propagation in dendrites of hippocampal pyramidal neurons. *Nature* **387,** 869–875.
18. Holmes W. R. and Levy W. B. (1990) Insights into associative long-term potentiation from computational models of NMDA receptor-mediated calcium influx and intracellular calcium concentration changes. *J. Neurophysiol.* **63,** 1148–1168.
19. Hubel D. H. and Wiesel T. N. (1965) Receptive fields and functional architecture in two nonstriate visual areas (18 and 19) of the cat. *J. Neurophysiol.* **28,** 229–289.
20. Jensen M. S., Azouz R. and Yaari Y. (1996) Spike after-depolarization and burst generation in adult rat hippocampal CA1 pyramidal cells. *J. Physiol.* **492,** 199–223.
21. Kisvárday Z. F., Martin K. A. C., Freund T. F., Maglóczky Zs., Whitteridge D. and Somogyi P. (1986) Synaptic targets of HRP-filled layer III pyramidal cells in the cat striate cortex. *Expl Brain Res.* **64,** 541–552.
22. Koch C. and Crick F. (1994) Further ideas about the neuronal basis of visual awareness. In *Large Scale Neuronal Theories of the Brain* (eds Koch C. and Davis J.), pp. 93–109. MIT, Cambridge, MA.
23. Larson J., Wong D. and Lynch G. (1986) Patterned stimulation at the theta frequency is optimal for the induction of hippocampal long-term potentiation. *Brain Res.* **368,** 347–350.
24. Laurent G. (1996) Dynamical representation of odors by oscillating and evolving neural assemblies. *Trends Neurosci.* **19,** 489–496.
25. Liley A. W. and North K. A. K. (1952) An electrical investigation of effects of repetitive stimulation on mammalian neuromuscular junction. *J. Neurophysiol.* **16,** 509–527.
26. Lisman J. (1997) Bursts as a unit of neural information: making unreliable synapses reliable. *Trends Neurosci.* **20,** 38–43.
27. Livingstone M. (1996) Oscillatory firing and interneuronal correlations in squirrel monkey striate cortex. *J. Neurophysiol.* **75,** 2467–2485.
28. Llinás R. R., Grace A. A. and Yarom Y. (1991) *In vitro* neurons in mammalian cortical layer 4 exhibit intrinsic activity in the 10 to 50Hz frequency range. *Proc. natn. Acad. Sci. U.S.A.* **88,** 897–901.
29. Llinás R. R., Ribary U., Joliot M. and Wang X.-J. (1994) Content and context in temporal thalamocortical binding. In *Temporal Coding in the Brain* (eds Buzsáki G., Llinás R. R., Singer W., Berthoz A. and Christen Y.), pp. 251–272. Springer, New York.
30. Madison D. V., Lancaster B. and Nicoll R. A. (1987) Voltage-clamp analysis of cholinergic action in the hippocampus. *J. Neurosci.* **7,** 733–741.
31. Mainen Z. F. and Sejnowski T. J. (1996) Influence of dendritic structure on firing pattern in model neocortical neurons. *Nature* **382,** 363–366.
32. Markram H. and Tsodyks M. (1996) Redistribution of synaptic efficacy between neocortical pyramidal neurons. *Nature* **382,** 807–810.
33. McCormick D. A. and Nowak L. G. (1996) Possible cellular mechanisms for arousal-induced higher frequency oscillations: acetylcholine and ACPD induce repetitive burst firing in visual cortical neurons. *Soc. Neurosci. Abstr.* **22,** 255.9.
34. Miles R. (1990) Synaptic excitation of inhibitory cells by single CA3 hippocampal pyramidal cells of the guinea-pig *in vitro*. *J. Physiol.* **428,** 61–77.
35. Mittmann T., Linton S. M., Schwindt P. and Crill W. (1997) Evidence for persistent Na^+ current in apical dendrites of rat neocortical neurons from imaging of Na^+-sensitive dye. *J. Neurophysiol.* **78,** 1188–1192.
36. Mize R. R., Marc R. E. and Sillito A. M. (eds) (1992) *GABA in the Retina and Central Visual System, Progress in Brain Research*, Vol. 90. Elsevier, Amsterdam.
37. Munk M. H. J., Roelfsema P. R., König P., Engel A. K. and Singer W. (1996) Role of reticular activation in the modulation of intracortical synchronization. *Science* **272,** 271–274.
38. Murthy V. N. and Fetz E. E. (1992) Coherent 25- to 35-Hz oscillations in the sensorimotor cortex of awake behaving monkeys. *Proc. natn. Acad. Sci. U.S.A.* **89,** 5670–5674.
39. Pinsky P. and Rinzel J. (1994) Intrinsic and network rhythmogenesis in a reduced Traub model for CA3 neurons. *J. comput. Neurosci.* **1,** 39–60.
40. Press W. H., Flannery B. P., Teukolsky S. A. and Vetterling W. T. (1989) *Numerical Recipes*. Cambridge University Press, Cambridge.
41. Rhodes P. A. and Gray C. M. (1994) Simulations of intrinsically bursting neocortical pyramidal neurons. *Neural Comput.* **6,** 1086–1110.
42. Ribary U., Ioannides A. A., Singh K. D., Hasson R., Bolton J. P. R., Lado F., Mogilner A. and Llinás R. R. (1991) Magnetic field tomography (MFT) of coherent thalamo-cortical 40-Hz oscillations in humans. *Proc. natn. Acad. Sci. U.S.A.* **88,** 11,037–11,041.
43. Schwindt P. and Crill W. E. (1995) Amplification of synaptic current by persistent sodium conductance in apical dendrites of neocortical neurons. *J. Neurophysiol.* **74,** 2220–2224.
44. Singer W. and Gray C. M. (1995) Visual feature integration and the temporal correlation hypothesis. *A. Rev. Neurosci.* **18,** 555–586.
45. Spain W. J., Schwindt P. C. and Crill W. E. (1991) Two transient potassium currents in layer V pyramidal neurones from cat sensorimotor cortex. *J. Physiol.* **434,** 591–607.

46. Steriade M. (1997) Synchronized activities of coupled oscillators in the cerebral cortex and thalamus at different levels of vigilance. *Cerebral Cortex* **7,** 583–604.
47. Steriade M., Curró Dossi R., Paré D. and Oakson G. (1991) Fast oscillations (20–40 Hz) in thalamocortical systems and their potentiation by mesopontine cholinergic nuclei in the cat. *Proc. natn. Acad. Sci. U.S.A.* **88,** 4000–4396.
48. Steriade M., Timofeev I., Dürmüller N. and Grenier F. (1998) Dynamic properties of corticothalamic neurons and local cortical interneurons generating fast rhythmic (30–40 Hz) spike-bursts. *J. Neurophysiol.* **79,** 483–490.
49. Stevens C. F. and Wang Y. (1995) Facilitation and depression at single central synapses. *Neuron* **14,** 795–802.
50. Stevens C. F. and Tsujimoto T. (1995) Estimates for the pool size of releasable quanta at a single central synapse and for the time required to refill the pool. *Proc. natn. Acad. Sci. U.S.A.* **92,** 846–849.
51. Storm J. F., Borg-Graham L. and Adams P. R. (1987) A passive component of the afterdepolarization (ADP) in rat hippocampal pyramidal cells. *Biophys. J.* **51,** 65a.
52. Stuart G. J. and Sakmann B. (1994) Active propagation of somatic action potentials into neocortical pyramidal cell dendrites. *Nature* **367,** 69–72.
53. Thomson A. M. and West D. C. (1993) Fluctuations in pyramid–pyramid excitatory postsynaptic potentials modified by presynaptic firing pattern and postsynaptic membrane potential using paired intracellular recordings in rat neocortex. *Neuroscience* **54,** 329–346.
54. Thomson A. M. and Deuchars J. (1995) Diverse pre- and post-synaptic properties of fast excitatory synapses. In *Excitatory Amino Acids and Synaptic Transmission* (eds Wheal H. V. and Thomson A. M.), pp. 145–172. Academic, London.
55. Thomson A. M. and Deuchars J. (1997) Synaptic interactions in neocortical local circuits: dual intracellular recording *in vitro*. *Cerebral Cortex* **7,** 510–522.
56. Thomson A. M., Deuchars J. and West D. C. (1993) Single axon excitatory postsynaptic potentials in neocortical interneurons exhibit pronouced paired pulse facilitation. *Neuroscience* **54,** 347–360.
57. Traub R. D. and Llinás R. R. (1979) Hippocampal pyramidal cells: significance of dendritic ionic conductances for neuronal function and epileptogenesis. *J. Neurophysiol.* **42,** 476–496.
58. Traub R. D., Jefferys J. G. R., Miles R., Whittington M. A. and Tóth K. (1994) A branching dendritic model of a rodent CA3 pyramidal neurone. *J. Physiol.* **481,** 79–95.
59. Tsodyks M. and Markram H. (1997) The neural code between neocortical pyramidal neurons depends on neurotransmitter release probability. *Proc. natn. Acad. Sci. U.S.A.* **94,** 719–723.
60. Turner R. W., Maler L., Deerinck T., Levison S. R. and Ellisman M. H. (1994) TTX-sensitive dendritic sodium channels underlie oscillatory discharges in a vertebrate sensory neuron. *J. Neurosci.* **14,** 6453–6471.
61. Varela J. A., Sen K., Gibson J., Fost J., Abbott L. F. and Nelson S. B. (1997) A quantitative description of short-term plasticity at excitatory synapses in layer 2/3 of rat primary visual cortex. *J. Neurosci.* **17,** 7926–7940.
62. Wang X.-J. (1993) Ionic basis for the intrinsic 40-Hz neuronal oscillations. *NeuroReport* **5,** 221–225.
63. Wang X.-J. and Buzsáki G. (1996) Gamma oscillations by synaptic inhibition in a hippocampal interneuronal network. *J. Neurosci.* **16,** 6402–6413.
64. Wang X.-J. and Rinzel J. (1992) Alternating and synchronous rhythms in reciprocally inhibitory model neurons. *Neural Comput.* **4,** 84–97.
65. Whittington M. A., Traub R. D. and Jefferys J. G. R. (1995) Synchronized oscillations in interneuron networks driven by metabotropic glutamate receptor activation. *Nature* **373,** 612–615.
66. Whittington M. A., Stanford I. M., Colling S. B., Jefferys J. G. R. and Traub R. D. (1997) Spatiotemporal patterns of γ frequency oscillations tetanically induced in the rat hippocampal slice. *J. Physiol.* **502,** 591–607.
67. Wilson M. and Bower J. M. (1992) Cortical oscillations and temporal interactions in a computer simulation of piriform cortex. *J. Neurophysiol.* **67,** 981–995.
68. Zucker R. S. (1989) Short-term synaptic plasticity. *A. Rev. Neurosci.* **12,** 13–31.

(*Accepted* 15 *May* 1998)